

Reconstruction of Undersampled Dynamic Images by Modeling the Motion of Object Elements

Claudia Prieto,¹ Philip G. Batchelor,² D.L.G. Hill,² Joseph V. Hajnal,³ Marcelo Guarini,¹ and Pablo Irarrazaval^{1*}

Dynamic MRI is restricted due to the time required to obtain enough data to reconstruct the image sequence. Several undersampled reconstruction techniques have been proposed to reduce the acquisition time. In most of these techniques the nonacquired data are recovered by modeling the temporal information as varying pixel intensities represented in time or in temporal frequencies. Here we propose a new approach that recovers the missing data through a motion estimation of the object elements (“obels,” or pieces of tissue) of the image. This method assumes that an obel displacement through the sequence has lower bandwidth than fluctuations in pixel intensities caused by the motion, and thus it can be modeled with fewer parameters. Preliminary results show that this technique can effectively reconstruct (with root mean square (RMS) errors below 4%) cardiac images and joints with undersampling factors of 8 and 4, respectively. Moreover, in the reconstruction process an approximation of the motion vectors is obtained for each obel, which can be used to quantify dynamic information. In this method the motion need not be confined to a part of the field of view (FOV) or to a portion of the temporal frequency. It is appropriate for dynamic studies in which the obels’ motion model has fewer parameters than the number of acquired samples. Magn Reson Med 57:939–949, 2007. © 2007 Wiley-Liss, Inc.

Key words: dynamic imaging; undersampling; reconstruction; obel; object element; motion

Dynamic MRI has become an important technique for studying the time behavior of many dynamic processes. Clinical applications include cardiac imaging (1), contrast-enhanced imaging (2), kinematics of joints and organs (3,4), functional MRI (fMRI) (5), and real-time interventional imaging (6). The simultaneous spatial and temporal resolution desired in these applications is limited due to data-acquisition time constraints. An important line of research in this area has been aimed at developing undersampling reconstruction techniques in k -space or in k - t space (7) without significantly compromising image quality. These techniques improve the acquisition time by reducing the number of acquired samples and estimating

the missing data by exploiting the high spatiotemporal correlation of dynamic sequences or from prior information.

Traditional approaches operate on a discrete k - t space and either treat each frame separately or consider the temporal information as time-varying pixel intensities represented in time or in temporal frequencies. Therefore, each pixel is considered in a constant position over time. These methods include keyhole (8,9), reduced encoding MR imaging with generalized-series reconstruction (RIGR) (10), reduced field of view (rFOV) (11), hybrid technique for dynamic imaging (12), unaliasing by Fourier-encoding the overlaps using the temporal dimension (UNFOLD) (13), sensitivity encoding incorporating temporal filtering (TSENSE) (14), k - t broad-use linear acquisition speed-up technique (k - t BLAST) (15), and reconstruction employing temporal registration (16). In contrast, in this work we are concerned not with the image pixels, but with the continuous position of the *object elements* (obel) through the dynamic sequence (17,18).

We define an obel as a piece of tissue of the object of interest whose intensity is constant over time. In this way, its temporal information is contained in its displacement or position through time. Obels can be arbitrarily defined, but for simplicity we usually use one or more pixels of the first frame of the sequence for each obel, and therefore they do not necessarily coincide with biological structures. The continuous position of all the obels that constitute an image will correspond to a motion model of the sequence.

The proposed method takes advantage of recent insights into non-rigid motion correction (19) and is based on two assumptions: 1) there is a high information redundancy in a fully sampled dynamic MR sequence, and 2) the displacement function of an obel in a dynamic sequence has a lower bandwidth than the fluctuations of intensity of stationary pixels caused by the movement. The first assumption suggests the existence of static or quasi-static parts of the image where the motion model is extremely simple, and that for those parts that do move more vigorously, the correlation between frames is very high and the motion model can be well approximated by a one-to-one transformation. The second assumption implies that the displacement of an obel can be described with fewer parameters than the number of time points in an equivalent dynamic sequence. This implication can be used to obtain a more accurate model of the motion or to increase the undersampling factor and therefore the temporal resolution. Accordingly, we are able to formulate a nonlinear system whose solution provides a static reference frame and a continuous position estimator for each obel in future frames.

¹Departamento de Ingeniería Eléctrica, Pontificia Universidad Católica de Chile, Santiago, Chile.

²Centre for Medical Imaging Computing, University College London, London, United Kingdom.

³Imaging Sciences Department, MRC Clinical Sciences Centre, Imperial College London, London, United Kingdom.

Grant sponsor: Fondo de Desarrollo en Ciencia y Tecnología; Grant number: 1030570; Grant sponsor: Royal Society.

*Correspondence to: Pablo Irarrazaval, Departamento de Ingeniería Eléctrica, Pontificia Universidad Católica de Chile, Vicuña Mackenna 4860, Macul, Santiago, Chile. E-mail: pim@ing.puc.cl

Received 20 September 2006; revised 5 February 2007; accepted 8 February 2007.

DOI 10.1002/mrm.21222

Published online in Wiley InterScience (www.interscience.wiley.com).

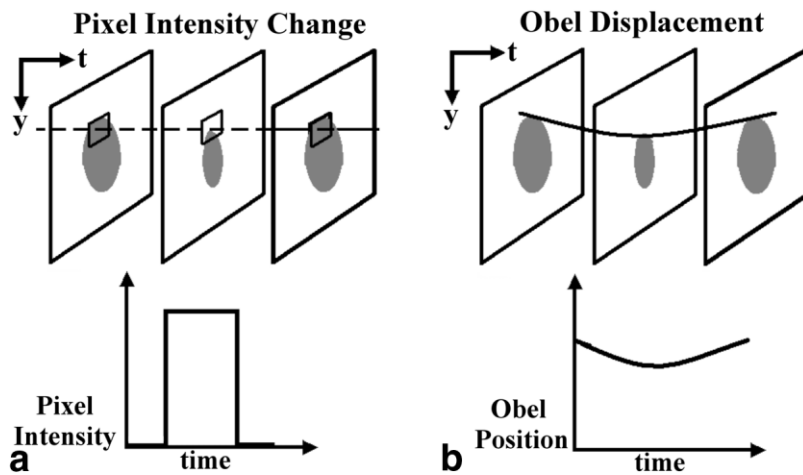


FIG. 1. Graphical comparison for the curves that describe the intensity fluctuation for a pixel near the edge of a moving object and the displacement of an obel in the same starting position. **a:** Time intensity fluctuation of the pixel. **b:** The obel's displacement through time.

Theoretically, a complete reconstruction of the dynamic sequence is possible if the degrees of freedom of the motion model are less than the number of acquired samples. In practice, the required samples are dependent on the efficacy and efficiency with which the associated nonlinear system can be solved. Just like reconstruction employing temporal registration (16), our method also generates an approximation of the motion vector field that can be used to assess relevant dynamic information, such as quantifying the movement of the myocardium.

This paper presents the proposed method and the results of its application to in vivo 2D images of the heart and joints. We provide a description of the relevant theoretical aspects as well as an experimental justification of our premises, a detailed description of the acquisition and reconstruction schemes, and finally an analysis of the results, which validate the proposed approach.

THEORY

Under the assumption that the obels' intensities do not change over time, it is possible to reconstruct a dynamic sequence of images given a reference frame of the sequence and the displacement through time of each obel from this reference frame. This statement also holds for undersampled dynamic images. In this case the solution of the inverse problem yields a fully sampled reference frame together with the associated motion model starting from undersampled acquisitions of the k - t space, allowing us to reconstruct a fully sampled dynamic sequence. The reconstruction is only feasible if the number of acquired samples exceeds the degrees of freedom of the motion model. To warrant a workable reconstruction and reach a high undersampling factor, the proposed method is based on two assumptions: 1) there is a high information redundancy in a fully sampled dynamic MRI sequence, and 2) the function of displacement of an obel in a dynamic sequence has a lower bandwidth than the fluctuations of pixel intensity caused by the movement. A brief rationale for these assumptions and a detailed description of the proposed reconstruction procedure are given below.

Justification of Assumptions

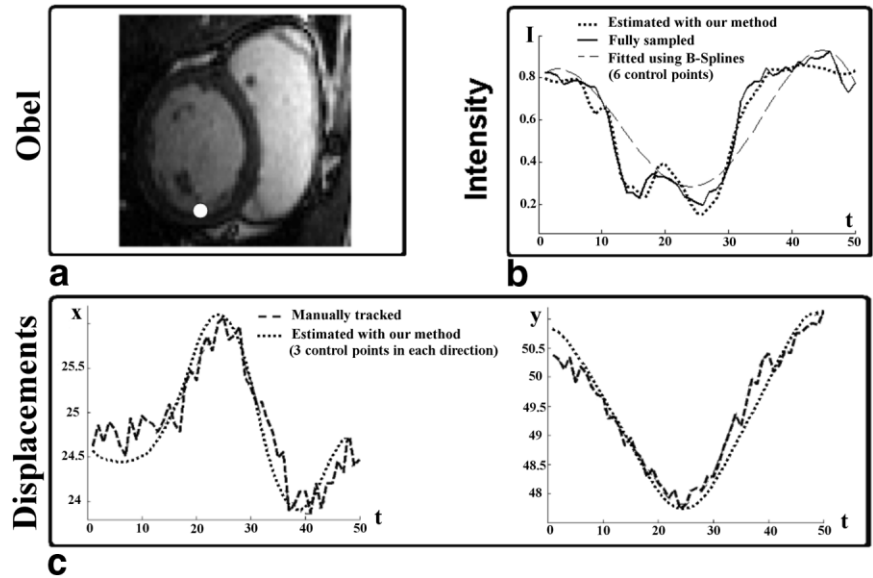
The high level of information redundancy between frames in dynamic MRI is evident if we consider the high degree

of undersampling attained using techniques such as k - t BLAST (15) and reconstruction employing temporal registration (16), among others. It is also noticeable from the sparse representation of the dynamic images in different domains, such as x - f space. It is difficult to assess the level of redundancy in dynamic sequences. However, a procedure described by Irrarazaval et al. (16) estimates a rough lower bound for the redundancy factor, which can be used to decide the maximum undersampling factor in a sequence, based on concepts of entropy and information theory. This limit is much higher than the undersampling factor we will use in this work.

The second assumption is easy to visualize if we consider a pixel near the edge of a moving object: the pixel will be inside of the object in some frames, and outside in others. As a result, the intensity of this pixel can change abruptly over time. On the other hand, an obel starting in the same position follows the moving object, describing a smooth continuous curve of displacement. It is reasonably clear that such a curve has lower bandwidth than a function describing a pixel intensity fluctuation, and hence can be formulated with fewer parameters. A graphical interpretation of this idea is depicted in Fig. 1.

To verify this second assumption we compared the displacement over time of a number of obels from 2D cardiac sequences with the intensity fluctuation of the pixels situated inside the obel in the reference frame. Figure 2 shows this comparison for a particular obel belonging to the left ventricular (LV) wall. The displacement over time of the obel was tracked manually from a fully sampled sequence, and estimated with our reconstruction from the undersampled dynamic data using B-splines with three control points. In order to demonstrate the benefit of tracking motion rather than intensity, pixel intensity fluctuation from fully sampled data was fitted using B-splines with six control points. This is compared with the fully sampled data and the result from our reconstruction from undersampled data using three control points for each displacement. Figure 2 shows that a better fit is obtained with displacements than with intensities, implying that more than six parameters would be necessary for the latter case. It is also clear from Fig. 2 that our reconstruction obtains a suitable approximation of the obels' motion.

FIG. 2. Real data comparison (2D dynamic sequence) for the displacement curves of a particular obel of the ventricular wall and the intensity fluctuation for the pixel in the same starting position. **a:** Obel on the ventricular wall. **b:** Time intensity fluctuation of the pixel. The B-spline used to fit the data has six parameters. **c:** Obel's displacement in the x and y directions through time. Each B-spline uses three parameters.



Reconstruction Procedure

Let \mathbf{m}_t be a discrete image of a dynamic sequence at time t . Under the assumption that obels do not change their intensity over time, if a reference frame \mathbf{m}_0 and the displacement of each obel whose initial position is defined in this frame are known, it is feasible to get any frame of the sequence. This is accomplished through a matrix multiplication in the image space using $\mathbf{m}_t = \mathbf{P}_t \mathbf{m}_0$ (19), where \mathbf{P}_t is the image transformation matrix that describes the spatial displacements over time for each obel initially defined in \mathbf{m}_0 . In other words, \mathbf{P}_t relates each obel in \mathbf{m}_0 with its new position in \mathbf{m}_t .

The image transformation matrices \mathbf{P}_t are permutation matrices that operate over a vectorized version of the reference frame. Their entries take values between zero and one to include the required permutation and interpolation processes. Interpolation is necessary to assign the continuous displacements of the obels to the discrete pixel positions and to ensure that there are no voids in image space. These matrices are large, sparse, and seldom invertible, even if the transformations are one to one between frames.

Although our method is based on the above image transformation, to improve efficiency it is written in the form of a spatial transformation as:

$$\mathbf{F}_t(\mathbf{x}) = \mathbf{x} + \mathbf{u}_t(\mathbf{x}) \quad [1]$$

where \mathbf{x} is the position vector in the reference frame, and \mathbf{u}_t is the vector representing the obels' displacement over all the spatial dimensions. \mathbf{F}_t^{-1} does not necessarily exist, but is much easier to compute or approximate. The linearity of the image space ensures that any spatial transformations \mathbf{F}_t lead to linear image transformations \mathbf{P}_t , such that for an image \mathbf{m}_0 the transformed image satisfies:

$$\mathbf{m}_t(\mathbf{y}) = \mathbf{P}_t \mathbf{m}_0(\mathbf{x}) = \mathbf{m}_0(\mathbf{F}_t^{-1}(\mathbf{y})) \quad [2]$$

where \mathbf{y} represents the vector position in any frame of the sequence \mathbf{m}_t in contrast to \mathbf{x} , which is defined in \mathbf{m}_0 . For each obel the spatial transformation $\mathbf{F}_t(\mathbf{x})$ can be parameterized and written as $\mathbf{F}(\mathbf{e})$, where \mathbf{e} is a matrix that defines the motion of all the obels. Each row of this matrix corresponds to a vector of parameters that describes the displacement of one particular obel initially defined in \mathbf{m}_0 . One vector is needed per obel to ensure an accurate description of any object and motion. We write $\mathbf{m}_t(\mathbf{m}_0, \mathbf{e})$ to state that it is possible to reconstruct \mathbf{m}_t from a known reference frame \mathbf{m}_0 and a set of parameters \mathbf{e} .

We now describe how to apply this representation to undersampled images. Let $B_t(\mathbf{k})$ represent the k - t space samples acquired using an undersampling pattern defined in matrix $S_t(\mathbf{k})$, where an entry of one means to sample in that position, and an entry of zero means not to sample in that position. Let $b_t(\mathbf{y})$ be the inverse Fourier transform of $B_t(\mathbf{k})$, which corresponds to the aliased image, \mathbf{W} be the Fourier transform matrix, and \mathbf{W}^H be its conjugate transpose. Then the equations equivalent to Eq. [2] in the k - t space domain for the undersampled case can be written as:

$$B_t(\mathbf{k}) = S_t(\mathbf{k}) \mathbf{W} \mathbf{m}_t(\mathbf{m}_0(\mathbf{x}), \mathbf{e}) \quad [3]$$

To improve solution stability the reconstruction is carried out in the image domain:

$$b_t(\mathbf{y}) = \mathbf{W}^H S_t(\mathbf{k}) \mathbf{W} \mathbf{m}_t(\mathbf{m}_0(\mathbf{x}), \mathbf{e}) \quad [4]$$

The reconstruction equation expressed in Eq. [4] corresponds to a nonlinear system in which $b_t(\mathbf{y})$, $S_t(\mathbf{k})$, and \mathbf{W} are known. The problem is to find the set of parameters \mathbf{e} and the reference frame \mathbf{m}_0 to satisfy this system of equations.

If the model has fewer degrees of freedom than the total number of acquired samples, the formulation allows a complete reconstruction of the image sequence. Letting Q be the undersampling factor, N_e the size of the matrix \mathbf{e} ,

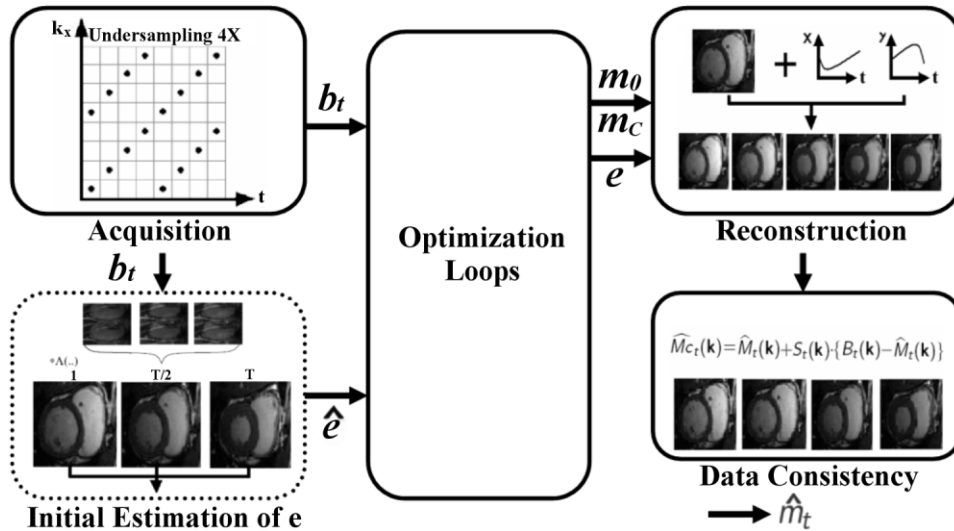


FIG. 3. Graphical summary of the proposed reconstruction algorithm. The acquired undersampled data are the input to two nested optimization loops, which determine the model motion of the obels, and can also be used to obtain an initial estimate of the parameters \mathbf{e} and speed up the optimization process. From the optimization loops we obtain the optimum values for \mathbf{m}_0 , \mathbf{m}_c , and \mathbf{e} , and thus we can reconstruct the whole image sequence. Finally, to ensure consistency in the reconstruction we use the estimated data only in the nonsampled positions of the k - t space.

and (N_d, N_t) the image dimensions, where N_d is the total number of voxels and N_t is the number of frames, the system in Eq. [4] has $N_d N_t / Q$ equations and $N_d + N_e$ unknowns. The equations correspond to the acquired samples, and the unknowns correspond to the number of pixels in the reference frame plus the number of parameters required to model the obels' motion over all the image dimensions. Consequently, in principle the system becomes fully determined if the following relation holds:

$$\frac{N_t}{Q} \geq 1 + \frac{N_e}{N_d} \quad [5]$$

This equation is used to compute the maximum allowed undersampling factor Q , given the image size, the number of frames, and the model employed to estimate the obels' motion. For example, with $N_t = 50$, $N_d = 256 \times 256$ and $N_e = 128 \times 128$ (one model every 4 pixels) $\times 4$ (control points per dimension) $\times 2$ (dimensions), the undersampling factor must be less than 16.6. If we consider as many obels as pixels in the reference frame, we need N_e / N_d parameters per obel to describe its motion.

Further accuracy can be achieved by employing more than one reference frame. This arrangement is convenient for 2D sequences in which some obels exit the slice. For instance, consider two reference frames (one at the beginning \mathbf{m}_0 and one in the middle of the sequence \mathbf{m}_c), then Eq. [4] becomes:

$$b_t(\mathbf{y}) = \mathbf{W}^H S_t(\mathbf{k}) \mathbf{W} m_t(m_0(\mathbf{x}), m_c(\mathbf{x}), \mathbf{e}) \quad [6]$$

which has to satisfy the relationship given by $N_t / Q \geq 2 + N_e / N_d$.

MATERIALS AND METHODS

The reconstruction algorithm was divided into three stages: 1) undersampling in k - t space, 2) modeling the obels' displacement, and 3) reconstruction and data consistency. This is shown schematically in Fig. 3.

According to the assumption that there exists enough information redundancy in a fully sampled dynamic sequence, k - t space was undersampled in a regular, uniform way, employing lattice sampling patterns like those used in k - t BLAST (15). The next step was to estimate the sequence reference frame and its corresponding motion model by solving the system in Eq. [6].

Finally, the whole sequence was reconstructed via spatial transformations, and the procedure for data consistency described in Ref. 16 was applied to ensure that the reconstruction results were consistent with the acquired samples. This final step is irrelevant if the solution reaches a global optimum.

Undersampling in k - t Space

If $M_t(\mathbf{k})$ represents the fully sampled time frames in k - t space, the undersampled acquisition $B_t(\mathbf{k})$ is represented as $B_t(\mathbf{k}) = S_t(\mathbf{k}) M_t(\mathbf{k})$, where $S_t(\mathbf{k})$ is the undersampling matrix. The undersampling patterns used in this work acquire $1/Q$ of the samples in each frame, with all samples collected every Q frames (similarly to k - t BLAST (15)).

Modeling the Displacement of Obels

From the undersampled data $B_t(\mathbf{k})$ or their image domain representation $b_t(\mathbf{y})$, we first estimated two reference frames of the sequence (\mathbf{m}_0 and \mathbf{m}_c) and the associated motion model. This was accomplished by solving the nonlinear system in Eq. [6] employing two nested optimization loops, as illustrated in Fig. 4. The inner loop estimated the values of $\hat{\mathbf{m}}_0$ and $\hat{\mathbf{m}}_c$ using the least-squares method to solve the overdetermined equation system:

$$b_t(\mathbf{y}) = \mathbf{W}^H S_t(\mathbf{k}) \mathbf{W} m_t(m_0(\mathbf{x}), m_c(\mathbf{x}), \hat{\mathbf{e}}) \quad [7]$$

where $\hat{\mathbf{e}}$ is known. The outer loop used $\hat{\mathbf{m}}_0$ and $\hat{\mathbf{m}}_c$ to estimate $\hat{b}_t(\mathbf{y})$ and to find the value of \mathbf{e} that minimized the mean square error between the acquired and the estimated sequence $\Delta \mathbf{b}$, i.e.:

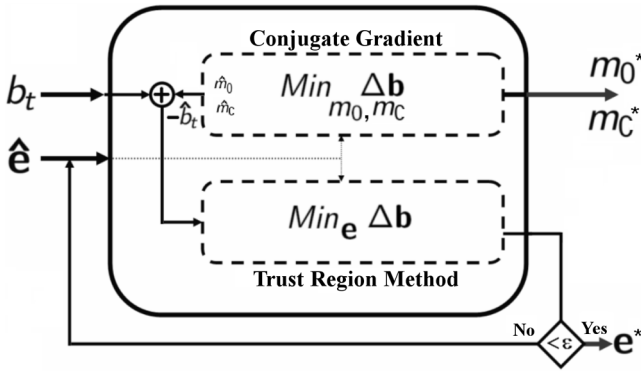


FIG. 4. Nested optimization loops. The inner loop finds the optimum \mathbf{m}_0 and \mathbf{m}_c for a given parameter \mathbf{e} . The outer loop finds the value of \mathbf{e} that minimizes the difference between the acquired data and the estimation obtained from the inner loop.

$$\begin{aligned} \text{Min}_e \Delta \mathbf{b} = \sum_{t=1}^{N_t} \|b_t(\mathbf{y}) - \hat{b}_t(\mathbf{y})\|_2 = \sum_{t=1}^{N_t} \|b_t(\mathbf{y}) \\ - \mathbf{W}^H S_t(\mathbf{k}) \mathbf{W} m_t(\hat{m}_0(\mathbf{x}), \hat{m}_c(\mathbf{x}), \mathbf{e})\|_2 \quad [8] \end{aligned}$$

In other words, for the inner loop \mathbf{e} is held constant and $\Delta \mathbf{b}$ is minimized as a function of \mathbf{m}_0 and \mathbf{m}_c , while for the outer loop the inner estimation of the reference frames is kept constant and the minimum of $\Delta \mathbf{b}$ is found as a function of \mathbf{e} .

Employing MATLAB (The MathWorks), the inner loop was solved using Least Square QR factorization (LSQR), which is a conjugate-gradient algorithm with good numerical properties (20). The algorithm allows explicit matrix multiplication to be replaced by a user-defined function, which is useful in our case since we can then work directly with $m_t(m_0(\mathbf{x}), m_c(\mathbf{x}), \hat{\mathbf{e}})$. The transpose product required in LSQR was approximated with the temporal average of \mathbf{b}_t , which was transformed by using the inverse spatial transformation as a function of \mathbf{e} . This substitution is highly efficient and allows a solution to Eq. [7] to be found almost instantaneously. The outer loop was solved by employing a trust-region method (the *fminunc* routine in MATLAB) together with an approximation of the analytic gradient of the objective function.

Each obel's displacement function was fitted using uniform quadratic B-splines for each spatial dimension. As a result, the displacement curves $\mathbf{u}_t(\mathbf{x})$ were parametrically represented as $\mathbf{u}(\mathbf{e})$ by employing the sum of basis functions, i.e.:

$$\mathbf{u}(\mathbf{e}_i) = \sum_{n=0}^{N_e/N_d-1} \mathbf{e}_i^n \mathbf{A}^n \quad [9]$$

where $\mathbf{u}(\mathbf{e}_i)$ is the displacement of the obel i , \mathbf{e}_i^n is the weight applied to the n^{th} B-spline base \mathbf{A}^n , and N_e/N_d is the number of parameters needed considering one obel per pixel. Each B-spline base is defined parametrically as $\mathbf{A}^n(s) = \mathbf{A}^0(s - n)$, a circularly translated copy of

$$\mathbf{A}_0(s) = \begin{cases} s^2/2 & \text{if } 0 \leq s < 1 \\ 3/4 - (s-3/2)^2 & \text{if } 1 \leq s < 2 \\ (s-3)^2/2 & \text{if } 2 \leq s < 3 \\ 0 & \text{otherwise} \end{cases} \quad [10]$$

As usual, the process terminates when changes are less than a specified tolerance or a predefined iteration limit is reached.

Reconstruction and Data Consistency

Once estimates of the optimum \mathbf{m}_0^* , \mathbf{m}_c^* , and \mathbf{e}^* are attained, the whole dynamic sequence $\hat{m}_t(\mathbf{y})$ is reconstructed using

$$\hat{m}_t(\mathbf{y}) = a_t m_0^*(\mathbf{F}_t^{-1}(\mathbf{e}^*)) + (1 - a_t) m_c^*(\mathbf{F}_t^{-1}(\mathbf{e}^*)) \quad [11]$$

where a_t is a weighting function for each reference frame. For the results presented in this paper, \mathbf{m}_c was selected to be the central image of the sequence. We employed the simple triangular weighting function $a_t = 1 - \Lambda(2t/N_t)$, which is appropriate for cases with cyclic motion.

To ensure consistency, data from sampled locations in k - t space are included instead of the estimated data, and the rest are modified slightly in order to be consistent with the sampled data (see Ref. 16 for details). This step is not necessary if the optimization is good enough, because the estimated and actually-sampled data values coincide.

Experiments

To test the proposed reconstruction algorithm, 2D dynamic sequences of the heart and a kinematic joint were used. Fully sampled images were acquired from volunteers on a Philips Intera 1.5T (cardiac images) and a Philips Gyroscan NT Intera 0.5T (joint images). Undersampling was simulated postacquisition by applying the desired lattice pattern to the acquired data. The results of our method were compared with the fully sampled images and with sliding-window (SW) reconstruction (21). The root mean square (RMS) error was used to quantitatively compare both reconstructions.

Cardiac Imaging

The algorithm was applied to reconstruct steady-state free precession (SSFP) dynamic (cine) sequences of two 2D sets of cardiac images. The scanner parameters used to obtain the fully sampled sequence for the first set of images (short axis) were as follows: 2D balanced fast field echo (B-FFE) cardiac-gated, TR/TE = 3 ms/1.46 ms, flip angle = 50°, FOV = 400 × 320 mm², resolution = 1.56 × 2.08 mm², slice thickness = 8 mm, acquisition matrix = 256 × 154, 50 frames, five-channel cardiac coil, and breath-hold duration close to 25 s. The parameters for the second set of images (long axis) were: 2D B-FFE cardiac-gated, TR/TE = 3.15 ms/1.57 ms, flip angle = 60°, FOV = 340 × 340 mm², resolution = 2.65 × 2.65 mm², slice thickness = 8 mm, acquisition matrix = 128 × 128, 25 frames, surface coil, and breath-hold duration close to 12 s. The complete acquired raw data sets were undersampled by simulating a lattice pattern in the phase-

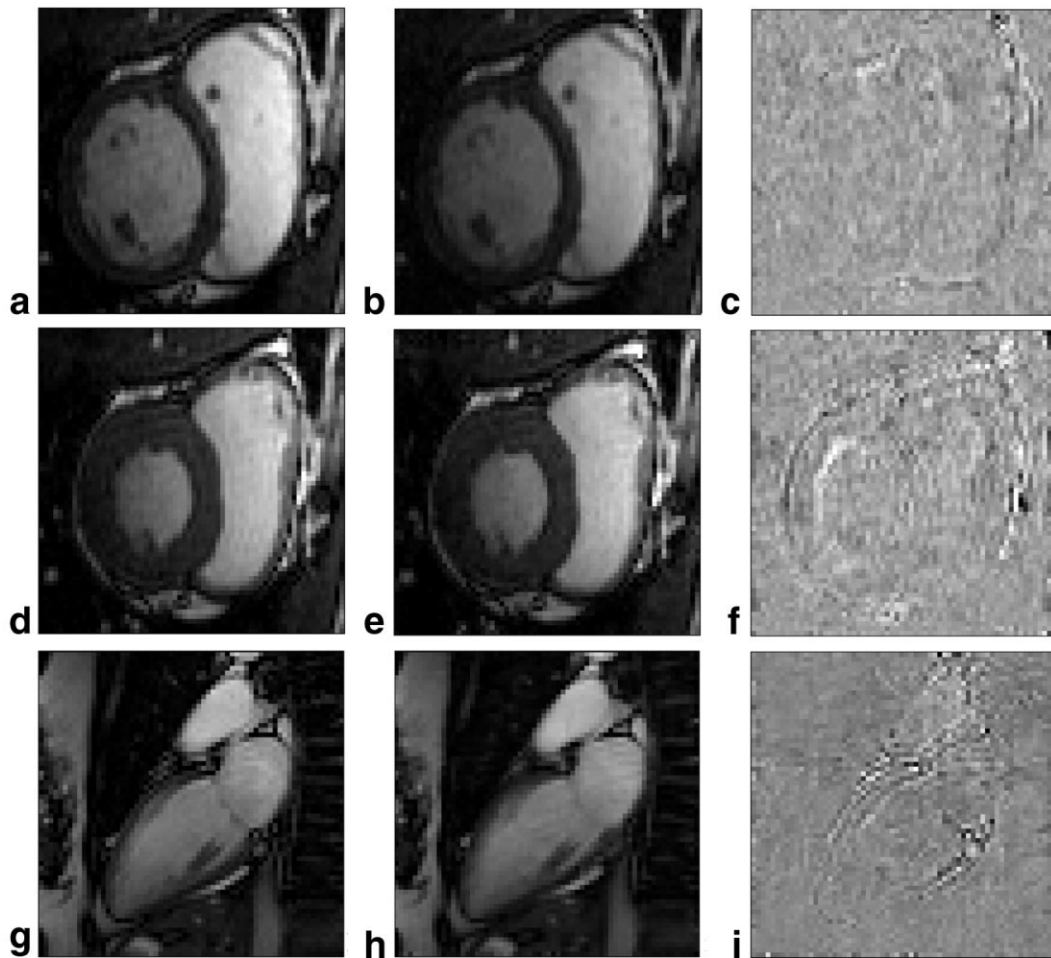


FIG. 5. Reconstructed images from 2D short- and long-axis cardiac sequence with a postacquisition undersampling factor of 4. The best (frame 1) and worst (frame 29) cases of a 50-frame sequence are shown for the short axis, and frame 5 of a 25-frame sequence is shown for the long axis. **a:** Fully sampled short-axis image frame 1. **b:** Reconstructed short-axis image frame 1 for $Q = 4$. **c:** Windowed difference between fully sampled and reconstructed images for short-axis image frame 1. **d:** Fully sampled short-axis image frame 29. **e:** Reconstructed short-axis image frame 29 for $Q = 4$. **f:** Windowed difference between fully sampled and reconstructed images for image frame 29. **g:** Fully sampled long-axis image frame 5. **h:** Reconstructed long-axis image frame 5 for $Q = 4$. **i:** Windowed difference between fully sampled and reconstructed images for image frame 5.

encoding direction. Undersampling factors of 4 and 8 were considered.

For both cases each pixel in the first reference frame was an obel. Three parameters per obel were used to describe their spatial displacements through the time sequence, where the complete set constituted the motion model. The model employed quadratic B-splines, and the beginning and end of the cardiac cycle were treated as coincident. An initial condition of **e** for the optimization process was obtained from a crude nonrigid registration of two frames from the sequence (i.e., the first and central frames) obtained via linear interpolation through time. To reduce the computational load, we concentrated the work in smaller regions of interest (ROIs), typically containing 2800–4500 obels and therefore 21000–31000 unknown variables.

Joint Imaging

An FFE dynamic sequence of the movement of the elbow was acquired with the following parameters: 2D FFE dy-

namic study, TR = 13.9 ms, TE = 8.54 ms, flip angle = 60°, FOV = 348 × 348 mm², resolution = 1.36 × 1.36 mm², slice thickness = 8 mm, acquisition matrix = 256 × 256, 24 frames, and a surface coil. The volunteer was asked to rotate her elbow between 0° and 50° and then between 50° and 0°, in a continuous and slow movement. Data were subsequently undersampled by a factor of 4. To ensure that the system of equations could be fully determined (Eq. [5]), we did not consider higher undersampling factors.

Considering each pixel in the reference frame as an obel, the motion model was fitted using quadratic B-splines and four parameters per obel in each spatial direction. To improve the convergence of the optimization process, we initialized using **e** such that it described a motion with a triangular function of time, with maximum displacements half way through the time series. The magnitude of this displacement was set at random independently for each obel. To reduce the computational load, we worked on an ROI of the image using about 2900 obels and 28000 variables.

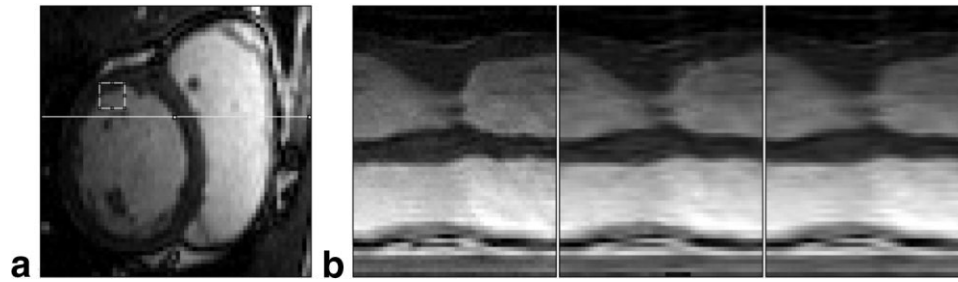


FIG. 6. Reconstructed images using the proposed and SW techniques from a 2D short-axis cardiac data set with a postacquisition undersampling factor of 4. The images show the time evolution of a line along the x -axis, indicated by the line in the fully sampled image. **a:** Fully sampled image. **b:** Evolution over time for the fully sampled image, proposed reconstruction, and SW reconstruction.

RESULTS

Cardiac Imaging

The reconstruction results for a factor of 4 undersampling of 2D cardiac images are shown in Fig. 5. Acquisitions of the short- and long-axis LVs were considered. For each case, selected fully sampled time frames are shown together with our reconstruction result and the windowed difference between both the original and reconstructed images, verifying the good agreement. Most of the aliasing is removed, and only slight spatial blurring is introduced. The difference images show that the main errors are due to small displacement of the edges, which could be solved with a better optimization of the motion's parameters. A comparison between the proposed technique and SW for an undersampling factor of 4 is shown in Fig. 6. The temporal evolution of the mean magnitude of differences over the whole image and over a small ROI (6×6 pixels) of the sequence is generally comparable to SW reconstruction, as shown in Fig. 7. Indeed, the difference images obtained in both cases are also similar. For an undersampling factor of 4, as illustrated, the proposed technique has a similar RMS reconstruction error to SW (1.26% for the proposed method and 1.10% for SW in the short-axis LV sequence, and 1.96% for the proposed method and 1.97% for SW in the large axis LV sequence, using normalized images).

The results of the reconstruction for an undersampling factor of 8 for our reconstruction and SW reconstruction are shown in Fig. 8 for one selected time frame. We have included in Fig. 8 the fully sampled data and the windowed difference with our reconstruction to confirm that they are in good agreement. These results also show (mainly in the edge of the LV) that the proposed algorithm improves the temporal resolution and reduces the aliasing and blurring in comparison with SW. Our method does introduce some temporal blurring because it imposes a "smooth" displacement for each obel; however, the low-pass filter effect of SW is stronger. This is illustrated in Fig. 9, which shows the plane y - t from a line passing through the LV for the proposed method and for SW reconstruction.

For an undersampling factor of 8, our method has a lower RMS error than SW reconstruction for the whole sequence (1.78% for the proposed method and 2.67% for SW using normalized images). This is because at high undersampling factors the main errors of SW (temporal

blurring and residual aliasing) are stronger than the main errors of our method (small displacement of the edges). This can be seen in Fig. 8, where the difference images with respect to fully sampled data for the proposed and SW reconstructions are shown in the spatial domain. Figure 10 shows the temporal evolution of the mean magnitude of differences over the whole image and over a small ROI (9×9 pixels). In this case the SW error is particularly strong at the beginning of the cardiac cycle.

Joint Imaging

The results of the reconstruction for an undersampling factor of 4 are shown in Fig. 11 for two selected time frames. We have included in Fig. 11a, b, d, and e the fully sampled data and our reconstruction to confirm that they are in good agreement, although the error in this case is stronger than that for the cardiac images. In this example the RMS error for our method is 4.04%, compared to

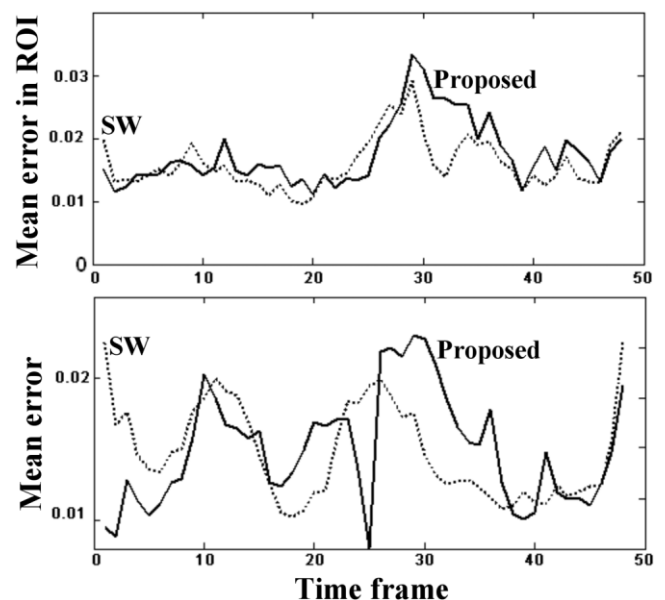


FIG. 7. Absolute mean error in the ROI and the whole sequence for the proposed and SW reconstructions as a function of time. The ROI is indicated by the square in Fig. 6a. The solid line shows the percent error for the proposed method, and the dashed line shows the percent error for SW reconstruction.

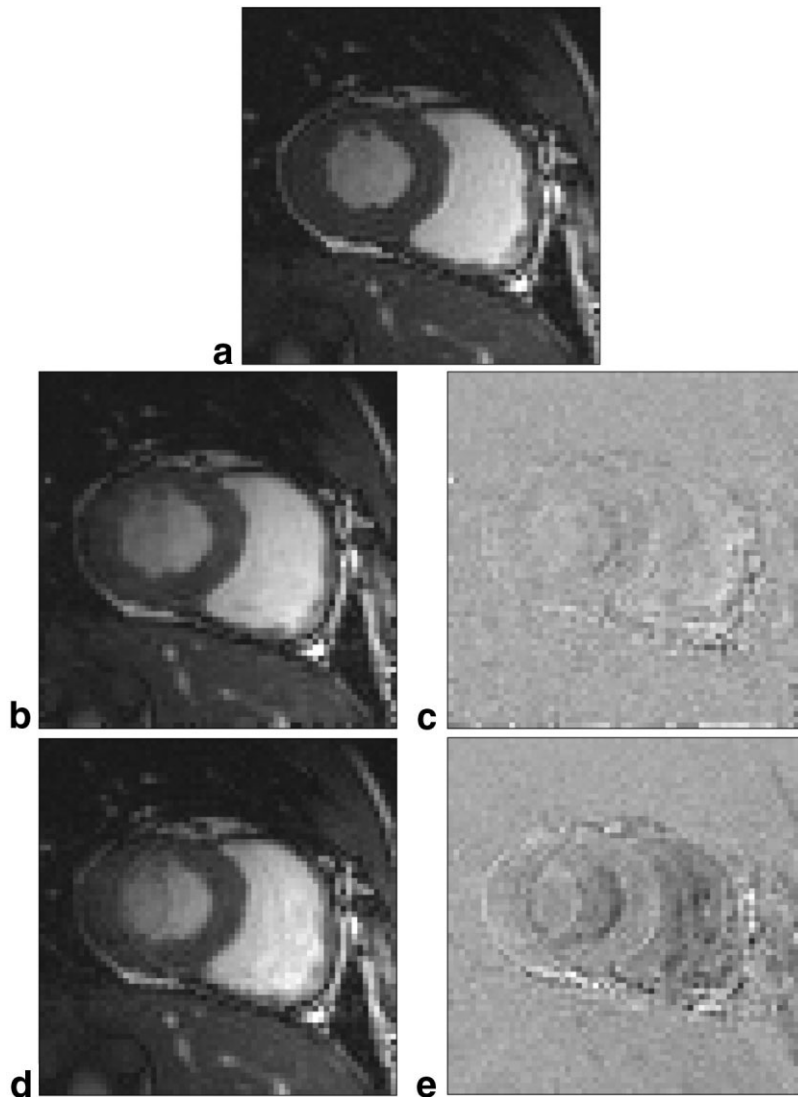


FIG. 8. Reconstructed images from a 2D short-axis cardiac sequence with a postacquisition undersampling factor of 8. Frame 26 of a 50-frame sequence is shown. **a:** Fully sampled image frame 26. **b:** Reconstructed image frame 26 for $Q = 8$ with our method. **c:** Windowed difference between a fully sampled image and our reconstruction for image frame 26. **d:** SW reconstruction image frame 26 for $Q = 8$. **e:** Windowed difference between a fully sampled image and SW reconstruction for image frame 26.

3.41% for SW reconstruction. As in the cardiac images, our method improves the temporal resolution and reduces the aliasing compared to SW, as shown in Figs. 11 and 12. Figure 11c and f show SW reconstruction for the same two selected time frames, while Fig. 12 shows the evolution over time for a line along the x-axis for the fully sampled data, our method, and SW reconstruction.

DISCUSSION

The results show that the proposed method is able to reconstruct undersampled dynamic sequences by employing motion estimation of each obel in continuous time. The motivation to use this strategy is that normally the displacement of an obel is smoother than the fluctuations

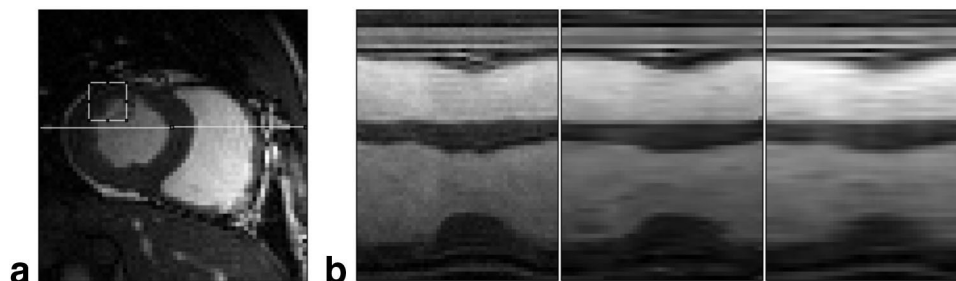


FIG. 9. Reconstructed images using the proposed and SW techniques from 2D short-axis cardiac data with a postacquisition undersampling factor of 8. The images show the time evolution of a line along the x-axis, indicated by the line in the fully sampled image. **a:** Fully sampled image. **b:** Evolution over time for the fully sampled image, proposed reconstruction, and SW reconstruction.

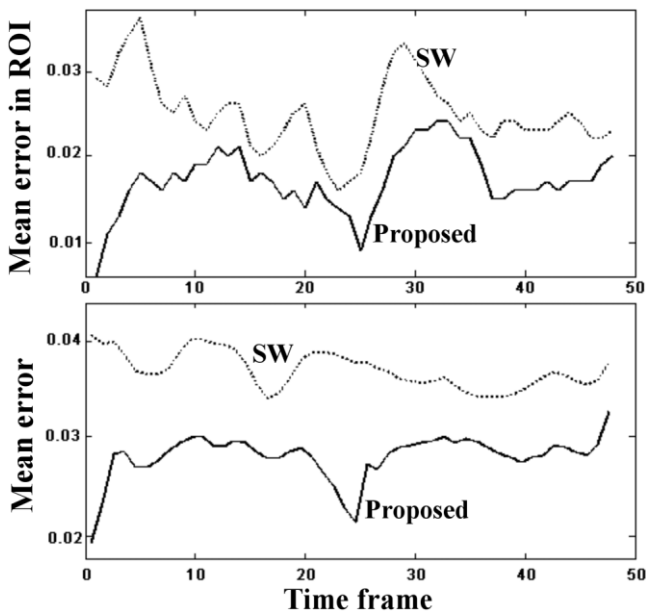


FIG. 10. Absolute mean error in the ROI and the whole sequence for the proposed and SW reconstructions as a function of time. The ROI is indicated by the square in Fig. 9a. The solid line shows the percent error for the proposed method, and the dashed line shows the percent error for SW reconstruction.

of pixel intensity caused by the movement, as was shown in Fig. 2.

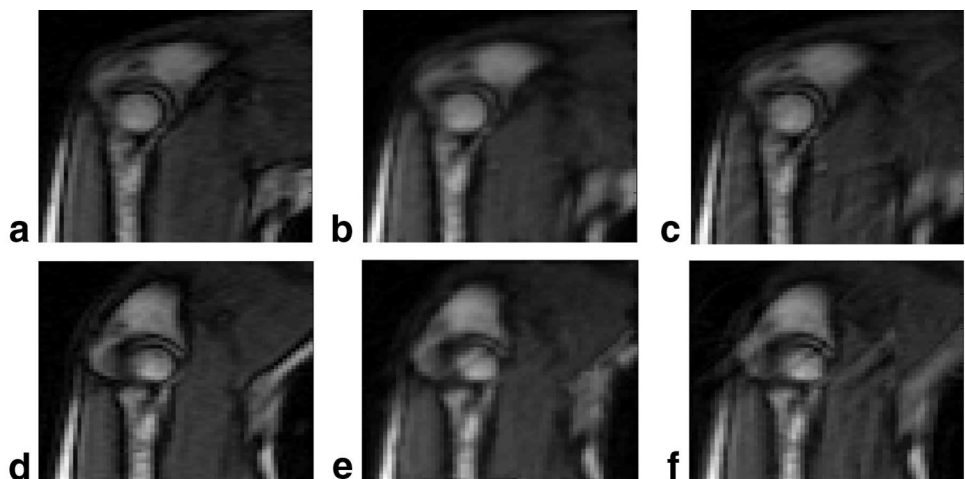
The reconstructed sequences exhibit a good spatial and temporal resolution, and are in good agreement with the fully sampled acquisitions. In general, edges are preserved and most of the aliasing is removed. Some spatial and temporal blurring is introduced because spatial interpolation and smooth continuous curves in time were considered. The interpolation is needed and incorporated in the spatial transformation F_t in order to assign the continuous displacements of the obels to the discrete pixel positions of the x - t image space. The main source of error of our method is the under- or overestimation of the displacements of obels on the edges of the object; however, this could be improved with a more accurate optimization.

The main advantage of the proposed method is that it does not require the motion to be confined to a part of the FOV or to a portion of the temporal frequency, and thus is independent of the sparsity of the x - f space. This was the case for the elbow reconstruction, in which most of the image was highly dynamic and presented considerable displacements. Other advantages of our method are that it is applicable to any kind of motion, it can be adapted to non-Cartesian trajectories and nonuniform undersampling patterns, and an approximation of the motion vectors for each obel in the image can be obtained as an additional result of the reconstruction process. The approximation of the motion can be used to quantify dynamic information, such as motion of the myocardium.

The high computational load of the current implementation is a limitation. Each reconstructed image in this paper took between 2 and 3 hr on a regular PC (Pentium IV, 1GB RAM). The processing time is strongly dependent on the image size, the number of obels defined in the reference frame, and the number of spline control points employed to fit the motion of each obel. In order to reduce the number of unknowns and thus the processing time, we can add constraints on the model motion. These restrictions could include 1) considering an obel to be formed of more than one pixel in the reference frame, 2) defining obels that coincide with biological structures and adding elastic restrictions of the tissue, 3) defining more obels in dynamic portions of the image or employing higher orders to estimate more dynamic obels, and 4) adding spatial continuity constraints in the movement of the obels. Another alternative to speed up the algorithm and improve its convergence is to use multiresolution optimization in the estimation of the parameter \mathbf{e} . We did not consider any of these alternatives in this paper, although we are working on the multi-resolution idea, which is promising for speeding up the optimization.

The proposed method has less RMS error compared to SW for an undersampling factor of 8 (1.78% for the proposed method and 2.67% for SW). This is not the case for an undersampled factor of 4 (1.26% for the proposed method and 1.10% for SW in short-axis acquisition, 1.96% for the proposed method and 1.97% for SW in long-axis acquisition, and 4.04% for the proposed method and

FIG. 11. Reconstructed images using the proposed and SW techniques from an elbow kinematic data set with a postacquisition undersampling factor of 4. Frames 3 and 14 of a 24-frame sequence are shown. **a**: Fully sampled image frame 3. **b**: Reconstructed image frame 3 for $Q = 4$. **c**: SW reconstruction for image frame 3 for $Q = 4$. **d**: Fully sampled image frame 14. **e**: Reconstructed image frame 14 for $Q = 4$. **f**: SW reconstruction for image frame 14 for $Q = 4$.



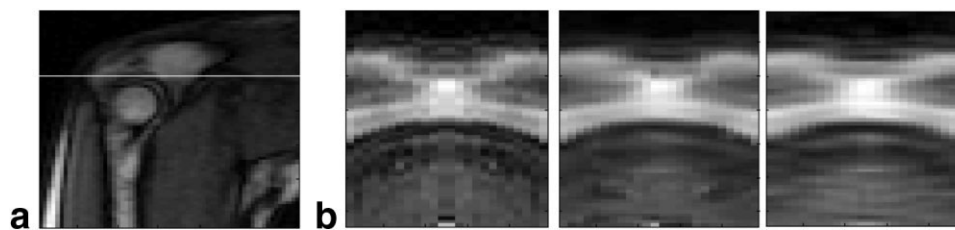


FIG. 12. Reconstructed images using the proposed and SW techniques from elbow kinematic data with a postacquisition undersampling factor of 4. The images show the time evolution of a line along the x-axis, indicated by the line in the fully sampled image. **a:** Fully sampled image. **b:** Evolution over time for the fully sampled image, proposed reconstruction, and SW reconstruction.

3.41% for SW in kinematic elbow acquisition); however, RMS error penalizes particularly strongly the displacement type of error produced by our method. Our method removes most of the aliasing and introduces less temporal blurring than SW, while retaining edges and a good signal-to-noise ratio (SNR).

The assumption that an obel does not change its intensity over time is strong and could be invalid in some situations, such as in 2D sequences where the movement is through the slice, in very noisy images, or when motion occurs within a nonuniform coil sensitivity field. Other situations where this assumption is not valid are dynamic contrast-enhanced studies and fMRI. The first problem can be overcome by employing more than one reference in order to consider strong temporal changes of intensity, and this problem should not be important in 3D images. To relax this assumption, which is necessary to identify each obel in the different frames, we could consider that the texture of an obel (which would require the obels to be formed by more than one pixel) and not its intensity is constant over time and use another measure of agreement (instead of the sum of the squared differences), such as the correlation coefficient.

For our method, the maximum undersampling factor depends on the image size and the model used to describe the motion of the obels. For the examples presented in this paper we used an undersampling factor of 4 for data sets with 25 or 50 time frames, and an undersampling factor of 8 with 50 time frames, with three or four parameters to describe the displacement of an obel in each spatial direction. There are situations in which the motion will be more complicated and would therefore require more parameters, restricting the feasible maximum undersampling factor. However, this was not the case in most of the applications we explored.

CONCLUSIONS

A method to reconstruct in vivo dynamic MRI sequences from undersampled data has been proposed. In contrast to the common approach in which temporal information corresponds to pixel intensity fluctuations, the proposed procedure recovers the missing data by motion estimation of obels. The supporting premise is that the obels' displacements have lower bandwidth than the fluctuations of pixel intensity caused by motion; therefore, their motion can be modeled with fewer parameters.

The performance of the method was tested using 2D cardiac sequences and sequences from a kinematic study of an elbow. Undersampling factors of 4 and 8 were investigated for the cardiac sequences, and a factor of 4 was investigated for the elbow. In all of the tests the method achieved good results and substantially eliminated the aliasing intrinsic to the undersampling while it minimized temporal blurring.

The method requires enough sampled data to faithfully describe the displacement of obels. Therefore, there is a trade-off between the maximum undersampling factor and the accuracy of the motion model. The high computational load of the current implementation is a limitation that will need to be improved for real applications of the algorithm.

The advantages of this method are that 1) it does not require the motion to be confined to a part of the FOV or to a portion of the temporal frequency, and 2) it can be adapted to non-Cartesian trajectories and nonuniform undersampling patterns. Furthermore, it obtains the vector field of motion, which can be used to quantify relevant dynamic information.

REFERENCES

- Earls JP, Ho VB, Foo TK, Castillo E, Flamm SD. Cardiac MRI: recent progress and continued challenges. *J Magn Reson Imaging* 2002;16:111–127.
- Song HK, Dougherty L, Schnall MD. Simultaneous acquisition of multiple resolution images for dynamic contrast enhanced imaging of the breast. *Magn Reson Med* 2001;46:503–509.
- Brossmann J, Muhle C, Schroder C, Melchert UH, Bull CC, Spielmann RP, Heller M. Patellar tracking patterns during active and passive knee extension: evaluation with motion-triggered cine MR imaging. *Radiology* 1993;187:205–212.
- Ichikawa T, Araki T. Fast magnetic resonance imaging of liver. *Eur J Radiol* 1993;187:205–212.
- Yang Y, Glover GH, van Gelderen P, Mattay VS, Santha AKS, Sexton RH, Ramsey NF, Moonen CTW, Weinberger DR, Frank JA, Duyn JH. Fast 3D functional magnetic resonance imaging at 1.5T with spiral acquisition. *Magn Reson Med* 1996;36:620–626.
- Kerr AB, Pauly JM, Hu B, Li KC, Hardy CJ, Meyer CH, Macovsky A, Nishimura DG. Real-time interactive MRI on a conventional scanner. *Magn Reson Med* 1997;38:355–367.
- Xiang QS, Henkelman RM. k-Space description for MR imaging of dynamic objects. *Magn Reson Med* 1993;29:422–428.
- Jones RA, Haraldseth O, Muller TB, Rinck PA, Oksendal AN. k-Space substitution: a novel dynamic imaging technique. *Magn Reson Med* 1993;29:830–834.
- van Vaals JJ, Brummer ME, Dixon WT, Tuithof HH, Engels H, Nelson RC, Gerety BM, Chezmar JL, den Boer JA. “Keyhole” method for accelerating imaging of contrast agent uptake. *J Magn Reson Imaging* 1993;3:671–675.
- Liang Z-P, Lauterbur PC. An efficient method for dynamic magnetic resonance imaging. *IEEE Trans Med Imaging* 1994;13:677–686.

11. Hu X, Parrish T. Reduction of field of view for dynamic imaging. *Magn Reson Med* 1994;31:691–694.
12. Parrish T, Hu X. Hybrid technique for dynamic imaging. *Magn Reson Med* 2000;44:51–55.
13. Madore B, Glover GH, Pelc NJ. Unaliasing by Fourier-encoding the overlaps using the temporal dimension (UNFOLD), applied to cardiac imaging and fMRI. *Magn Reson Med* 1999;42:813–828.
14. Kellman P, Epstein FH, McVeigh ER. Adaptive sensitivity encoding incorporating temporal filtering (TSENSE). *Magn Reson Med* 2001;45:846–852.
15. Tsao J, Boesiger P, Pruessmann KP. k-t BLAST and k-t SENSE: dynamic MRI with high frame rate exploiting spatiotemporal correlations. *Magn Reson Med* 2003;50:1031–1042.
16. Irarrazaval P, Boubertakh R, Razavi R, Hill D. Dynamic three-dimensional undersampled data reconstruction employing temporal registration. *Magn Reson Med* 2005;54:1207–1215.
17. Prieto C, Guarini M, Hill D, Boubertakh R, Batchelor P, Hajnal J, Irarrazaval P. Undersampled dynamic data reconstruction based on object motion estimation. In: Proceedings of the 13th Annual Meeting of ISMRM, Miami Beach, FL, USA, 2005 (Abstract 2302).
18. Prieto C, Mir R, Batchelor P, Hill DLG, Guarini M, Irarrazaval P. Reconstruction of undersampled dynamic images by modeling the motion of object elements. In: Proceedings of the 14th Annual Meeting of ISMRM, Seattle, WA, USA, 2006 (Abstract 687).
19. Batchelor PG, Atkinson D, Irarrazaval P, Hill DLG, Hajnal J, Larkman D. Matrix description of general motion correction applied to multishot images. *Magn Reson Med* 2005;54:1273–1280.
20. Paige C. LSQR: an algorithm for sparse linear equations and sparse least squares. *ACM Trans Math Software* 1982;8:43–71.
21. d'Arcy JA, Collins DJ, Rowland IJ, Padhani AR, Leach MO. Applications of sliding window reconstruction with Cartesian sampling for dynamic contrast enhanced MRI. *NMR Biomed* 2002;15:174–183.